

CFD MODELLING OF ALUMINA SLURRY HEAT EXCHANGER HEADERS: (i) COMPARISON OF CFD APPROACHES

Klaus BREMHORST¹ and Matthew BRENNAN²

¹School of Engineering, The University of Queensland, Brisbane, Queensland, 4072, AUSTRALIA

²JK Tech Pty Ltd, The University of Queensland, Isles Rd, Indooroopilly, Queensland, 4068, AUSTRALIA

ABSTRACT

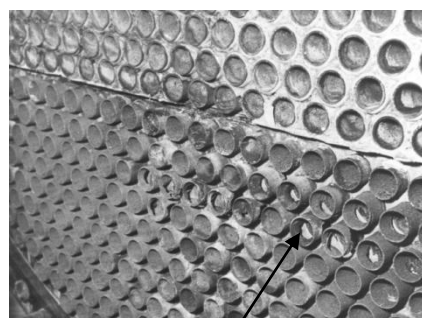
New flow modelling strategies have been developed for flow simulation in the inlet header and between passes header of side entry shell and tube heat exchangers used in alumina plants for heat recovery. The traditional approach of treating the tube bundle as a porous plug observing Darcy's friction law has been replaced by modelling of all tubes individually and application of an inertial model for flow resistance. Use of symmetry has been abandoned and shows that a symmetrical expansion of flow from the inlet nozzle into the inlet header no longer results. Areas of high angle of flow into tubes, variations of mass flow and vorticity distributions across tube sheets and a flow component across what is a geometrical symmetry plane are identified.

NOMENCLATURE

g	gravitational constant
k	turbulent kinetic energy
p	pressure
S_{ij}	mean strain rate tensor
$\overline{u_i, u_j}$	mean velocity in tensor notation
$\overline{u_i u_j}$	temporal average of fluctuating velocities
x_i, x_j	coordinates in tensor form
ρ	density
μ	dynamic viscosity
ω	specific dissipation rate
Ω_{ij}	mean vorticity tensor

INTRODUCTION

Production of alumina from bauxite generally uses the Bayer process which involves dissolving the aluminium in bauxite, in a hot caustic solution and in a high pressure digester. Considerable heat recovery is achieved where flash steam from the digester product is used to pre-heat the feed. In early plant designs, the caustic solution was heated separately but in recent designs the bauxite is mixed with the caustic before heating and the slurry is heated. Shell and tube heat exchangers, typically constructed of mild steel, are commonly used with both direct slurry heating and the older technology of caustic heating. Due to the build up of scale, regular descaling with an acid wash is undertaken in order to restore good heat transfer. During acid cleaning, the protective oxide layer on the mild steel is removed thus leading to enhanced metal loss until the protective layer is restored. Damage caused is illustrated in Figure 1.



Metal loss through full tube thickness

Figure 1. First pass inlet of four pass shell and tube heat exchanger

The electrochemical flow processes involved are not well understood and the concern in existing alumina plants is what happens if throughput is increased to give a higher yield. While mass transfer processes are often flow Reynolds number dependent with higher Reynolds numbers leading to higher metal loss (flow accelerated corrosion), little evidence exists in support of such a hypothesis. As corrosion is an electrochemical process, it should be possible to reduce it by chemical means. The use of liquor aeration or even oxygenation has been examined in the laboratory (Kear and Bremhorst, 2008a and 2008b) but found to be beneficial only under limited conditions which may not be met in an alumina plant. However, the dominant factor isolated so far which affects metal loss at tube inlets is the pattern of flow into tubes. Maximum metal loss generally occurs where flow into tubes is at a large angle to the tube axis leading to possible flow separation as shown in Figure 2 (Elvery and Bremhorst, 1996). Few predictive models exist for the electrochemical processes (Nešić, 2006) thus leaving the most promising line of enquiry to be the search for flow into tubes being as near to axial as possible (Bremhorst and Lai, 1979 and Lai and Bremhorst, 1979). Flow modifiers proposed by these authors have had extensive testing in the plant environment with dramatic improvement in tube life.

Since the introduction of slurry heating, the solid phase has introduced new problems due to solids build up at the inlet end of passes. Little is known about the mechanisms involved in the build up but the aim is to avoid tube areas with low flow velocities. The first area of major concern is the inlet header as already discussed above in the context of the studies by Bremhorst and Lai (1979) and

Lai and Bremhorst (1979). The second area of interest is in the header spaces connecting one pass to another where a typical area ratio of 1:3 exists of tube flow area to header area giving uncontrolled flow expansion. This second issue is of importance with slurry heaters where a solid phase of some 10-12% by volume of solids exists. Under unfavourable flow conditions, solids separate out from the liquid phase and cause build up and blockage of tubes in the next pass. Consequently, in the current investigations, the aim has been to model both these header areas in order to help identify areas leading to rapid wear and/or blockages by solid build up. Advances in computational resources since the seventies and the development of reliable turbulence models, has allowed the replacement of experimental work in the search for ideal flow patterns applying to this particular geometry of heat exchanger (Bremhorst and Flint, 1988, 1989 and 1991, Nešić, 2006).

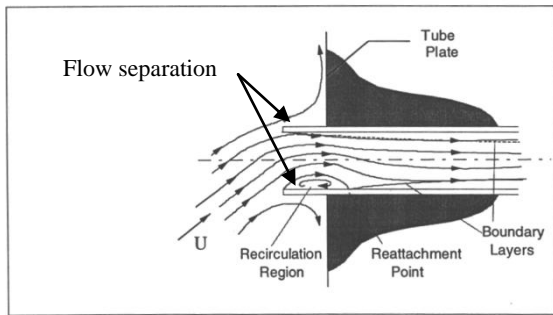


Figure 2. Flow separation at tube inlet

The modelling approaches used by these authors arose from the early limitations of computational resources necessitating the representation of the tube bundle by a porous plug with a resistance given by Darcy's law and use of symmetry to reduce the number of computational nodes. Although results were generally quite representative, the opportunity now exists to test the effect of different models and to considerably refine modelling thus leading to a better understanding of the flow processes.

Whilst the main focus of this work is to investigate the hydrodynamics of slurry heaters used in the Bayer alumina process, the results from the investigation have application in existing plants where the older technology of caustic only heating continues to be used and in other areas where heat exchangers of this type are used with corrosive materials.

MODEL DESCRIPTION

Physical Model

The simulations reported here are of a side entry, parallel pass geometry shown in Figure 3. A single phase liquor feed rate of $1640 \text{ m}^3\text{h}^{-1}$ with density 1410 kg.m^{-3} (equivalent to 10% by volume of alumina) and dynamic viscosity of $0.005 \text{ kg.m}^{-1}\text{s}^{-1}$ was assumed. The first pass geometry is completed by addition of the tube zone for which different modelling approaches are discussed below. Tubes are flush with the tubesheet in order to limit the number of computational nodes.

Flow Modelling

Continuity and momentum equations were Reynolds averaged (equations (1)- (3)) and the SST-k- ω turbulence model was used (equations (4) – (5)). The time dependent

form was used to help with the solution process. Results are for the final steady state solution.

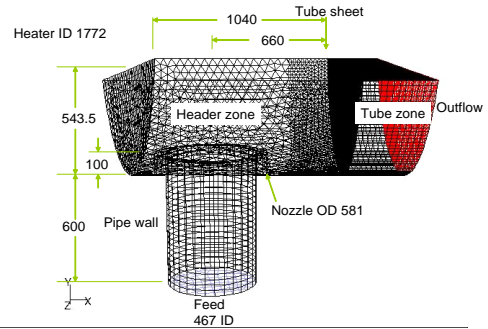


Figure 3. Dimensioned and meshed geometry for inlet header – dimensions are in mm

$$\frac{\partial u_i}{\partial x_i} = 0 \quad (1)$$

$$\frac{du_i}{dt} + u_j \frac{\partial u_i}{\partial x_j} = -\frac{1}{\rho} \frac{\partial p}{\partial x_i} + \frac{\partial}{\partial x_j} (2(v + v_t)S_{ji}) + g_i \quad (2)$$

$$v_t = k / \omega \quad (3)$$

$$\begin{aligned} \frac{\partial}{\partial t} k + u_j \frac{\partial}{\partial x_j} k = & -\overline{u_i u_j} \frac{\partial u_i}{\partial x_j} - \beta^* k \omega \\ & + \frac{\partial}{\partial x_j} \left((v + \alpha^* v_t) \frac{\partial}{\partial x_j} k \right) \end{aligned} \quad (4)$$

$$\begin{aligned} \frac{\partial}{\partial t} \omega + u_j \frac{\partial}{\partial x_j} \omega = & -\alpha \frac{\omega}{k} \overline{u_i u_j} \frac{\partial u_i}{\partial x_j} - \beta \omega^2 \\ & + \frac{\partial}{\partial x_j} \left((v + \alpha v_t) \frac{\partial}{\partial x_j} \omega \right) \end{aligned} \quad (5)$$

$$\text{where } \alpha = \frac{13}{25}, \quad \alpha^* = \frac{1}{2}, \quad \beta = \frac{9}{125} \left[\frac{1 + 70X_\omega}{1 + 80X_\omega} \right]$$

$$\beta^* = \frac{9}{100} \left[\frac{1 + 680X_k^2}{1 + 400X_k^2} \right] \text{ for } X_k > 0 \text{ otherwise } = \frac{9}{100}$$

$$X_k = \frac{1}{\omega^3} \frac{\partial k}{\partial x_j} \frac{\partial \omega}{\partial x_j} \text{ and } X_\omega = \left| \frac{\Omega_{ij} \Omega_{jk} S_{ki}}{(\frac{9}{100} \omega)^3} \right|$$

The header and inlet nozzle geometry (see Figure 3) are symmetric about a plane perpendicular to the pass separation. Previous CFD studies have assumed that the flow is symmetric about this plane and computed only one half of the inlet pass to minimise the computation. However in this work the full inlet header geometry has been simulated, because simulation of only half of the header forces symmetry of the flow which may not occur in reality.

Recent experimental studies of a step expansion flow between infinite parallel plates (Escudier et al (2002), Sugawara et al (2005), Duwig et al (2008) and Drikakis (1997)) have shown that the flow does not expand symmetrically and attaches preferentially to one side of the expansion, with the data suggesting that a flow reversal may even form. In the side entry parallel pass header, the flow expands rapidly from the inlet nozzle into a space which is not axisymmetric. It is untested whether or not a symmetrically expanding flow results. Experimental data of Bremhorst and Lai (1979) certainly

lack perfect symmetry which so far has been attributed to experimental variability but in light of these recent observations with the step parallel plate expansions, may in fact be a real flow characteristic.

Tube Zone Modelling – “porous plug” vs “with tubes”

Initially the tube zone was represented by a porous plug extension to the header with a Darcy’s law resistance (resistance proportional to velocity) and a one directional diffusion coefficient to give a pressure drop of some 46 kPa (similar to plant values for the tube bundle). As the tube resistance is in reality proportional to the square of tube flow velocity (inertial model), this option was tested for effects on flow distribution across the tube sheet face.

Subsequently, the geometry was modified so that the tube sheet and the first 0.9 m of each tube in the tube bundle was simulated (the “with tubes” approach). In this approach the first 0.6 m of each simulated tube has been made a free turbulent flow region and the last 0.3 m was made a porous zone where the porosity was adjusted to give a pressure drop from the tube plate equal to the typical pressure drop along a first pass tube bundle.

The “with tubes” approach introduces several important differences and enhances the modelling. Firstly the tube sheet has been introduced as a wall boundary condition and momentum transfer by shear to the tube sheet is introduced into the simulation which is not possible with the porous plug approach. Secondly flow separation within individual tube entrances and flow mal-distribution down particular tubes due to the hydrodynamic effects in the header can now be modelled. Finally in the “porous plug” approach, the axial velocity which determines the pressure drop is determined by the product of the flow velocity magnitude and its angle relative to the tube axis. With the “with tubes” approach, a given axial velocity (which again determines the pressure drop) is a function of flow velocity magnitude, its angle relative to the tube axis and the azimuthal angle of the velocity vector because the tube array about a given tube is not axisymmetric.

The tube bundles in heaters of this type are typically 8 m in length. Simulating only the first 0.6 m of each tube in the bundle as a free turbulent flow is a modelling compromise, however the correct over all pressure drop can be obtained by adjusting the porosity in the second 0.3 m porous zone while giving 18 tube diameters to simulate entrance effects and flow development along the tubes.

Numerical Details

The grid was generated in Gambit and the cases were solved with FLUENT Version 6.2.16. High order discretization of the equations was used; PRESTO was used for pressure, 3rd order MUSCLE on all other equations and SIMPLE for the pressure-velocity coupling. Grid dependence was tested. Grid refinement near the tubesheet was applied, as seen in Figure 3, until solutions changed little from one refinement to the next. A 20 mm unstructured tetrahedral mesh in the header was found to be satisfactory for both the “porous plug” and “with tubes” approach but with the “with tubes” approach, a 7.5 mm tri surface mesh was applied at the tube sheet and tube entrances. A velocity inlet boundary condition was used at the inlet pipe boundary and an outflow boundary condition was used at the header outlet with the “porous plug” model. Pressure outlet boundary conditions were used on tube outlets in the “with tubes” model.

RESULTS

“Porous Plug” Approximation for Tubes – Inlet Header

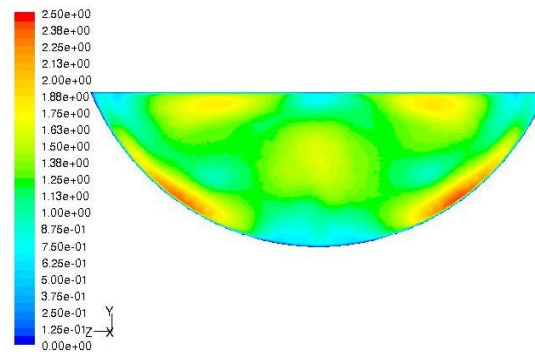


Figure 4. Contours of velocity magnitude at tube sheet

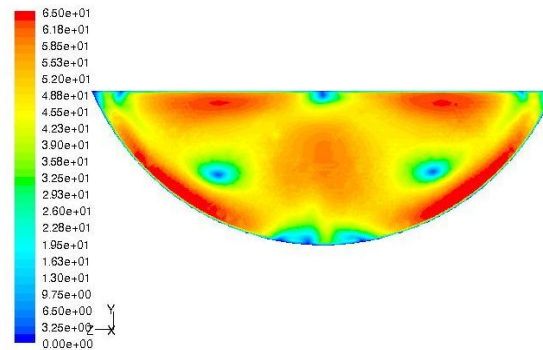


Figure 5. Contours of flow angle relative to tube axis at tubesheet

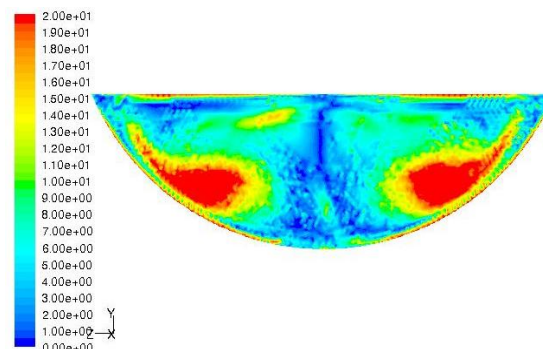


Figure 6. Contours of vorticity aligned with tube axis

Figures 4-6 show contours of flow conditions at the tube sheet for the “Porous plug” approximation. Contours of velocity magnitude, Figure 4, are relevant to impact effects of flows if particles are present in the flow while contours of velocity angle relative to the tube axis, Figure 5, give an indication of likelihood of flow separation inside and outside of in tubes. Velocity magnitude and angle determine flow velocity through the tubes and hence mass flow distribution across the tube sheet. Contours of the component of vorticity aligned with the tube axis, Figure 6, give further insight into the flow structure. The existence of the well defined flow distributions is attributable to the side entry flow which leads to a well defined vortex structure.

“With Tubes” Approximation for Tubes

The “with tubes” approach used the geometry of Figure 3 but with the tube zone replaced by an array of 274 tubes of 33 mm ID and 0.9 m in length and on a 47.625 mm triangular pitch. As described earlier the last 0.3 m of each

tube was modelled as a porous zone with the porosity adjusted to give an overall pressure drop of 46 kPa. Initial simulations used a Darcy law approximation for the porous plug as mass flow distributions across the tube sheet do not differ significantly. Flow quantities are displayed 10 mm upstream of the tube sheet in order to reduce the variability of results due to mass flow variations between tubes.

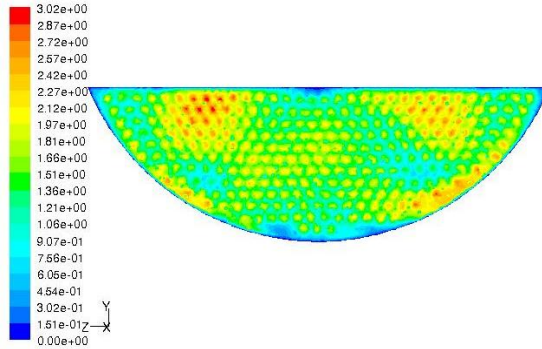


Figure 7. Velocity magnitude “with tubes” case

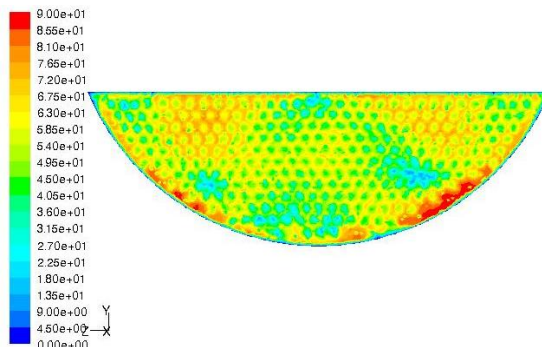


Figure 8. Flow angle relative to tube axis “with tubes” case

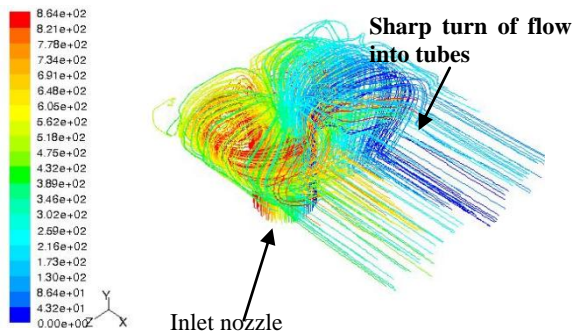


Figure 9. Path lines “with tubes” case

Comparison of Figure 4, Figure 7 and Figure 5, Figure 8 shows that there is a significant asymmetry in the flow simulated by the “with tubes” case and which is not seen in the “porous plug” case. Considerable effort has gone into ensuring that this is not a convergence or grid problem. In the “with tubes” case higher velocity magnitudes are noticed because the space between tubes does not carry mass flow as is the case with the porous plug approach. Flow angles are also larger in the “with tubes” case, Figure 5 and Figure 8. The reason for this increased angle is due to the fact that with tubes, flow occurs along the tube sheet between tubes and this then turns sharply into the tubes, Figure 9.

Figure 10 shows that the lack of symmetry is due to cross-flow from one half of the inlet header to the other half. Figure 10 also shows the very sharp angles of flow at the

entry into the tubes. Referring back to Figure 9, it can be seen that there is a strong cross flow down the shell on each side of the header and these two cross flows collide at the plane of header symmetry ($z=0$). Whilst the flow turns and goes into the tubes, it is not unreasonable that with the momentum associated with these two cross flows, the flow “gives” with one flow separating from the shell and going over the top of the other, leading to a flow asymmetry.

The solutions obtained are not unique and, depending on the manner in which solutions were commenced, a mirror image solution has been obtained. This is to be expected as there is no asymmetric feature in the inlet flow or the geometry or the solution process which might favour one solution over another. What is problematical is whether each mirror image is a stable state in the real flow for which there is an approximately equal probability of occurrence or whether each is a meta-stable condition between which the real flow switches over time.

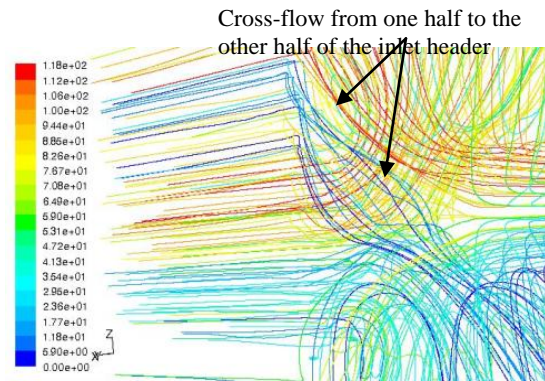


Figure 10. Pathlines “with tubes” case as seen through the shell from the inlet nozzle on the right

Application of results obtained must, therefore, be interpreted by including the mirror image about the line of geometric symmetry as well as solutions obtained from different starting conditions. As Eqs. (2), (4) and (5) are time dependent, unsteady RANS solutions are obtained where the time varying flow variables can be viewed as representative of the larger flow structures which vary with time while the finer structures are modelled by the turbulence model. Although in the present work, the time element has been retained in the equations in order to assist convergence, if large scale structures exist, instantaneous solutions will continue to vary about the steady state means. Consequently, an indication of the fuller extent of regions of high flow angle or low tube inlet velocity will become evident. A more accurate approach is to apply a large eddy simulation which is given below.

Static Pressure Drops

“With tube” simulations also yield the static pressure profile within tubes. Figure 11 shows that each tube has a relatively large entrance loss. Due to varying angles of approach of the flow into the tubes, entry losses vary across the tube sheet from 11 kPa (blue) down to only 3 kPa (red) as seen from Figure 12, for a header pressure of around 46 kPa. Comparison of Figure 8, Figure 8 and Figure 12 indicates that regions of high flow angle correspond to regions of low pressure inside the tubes which is indicative of high entry losses associated with flow separation.

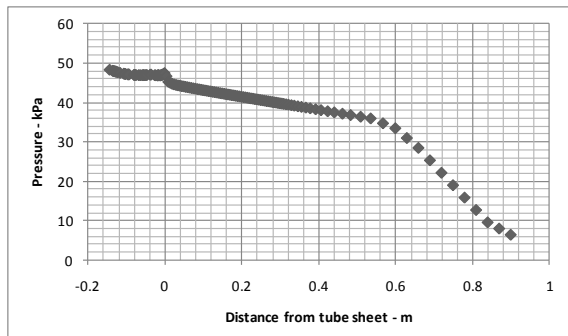


Figure 11. Simulated pressure drop along central tube to porous zone (at $y=0.294\text{m}$, $z=0.0\text{m}$). Tube entrance is at the tube sheet position of 0 m .

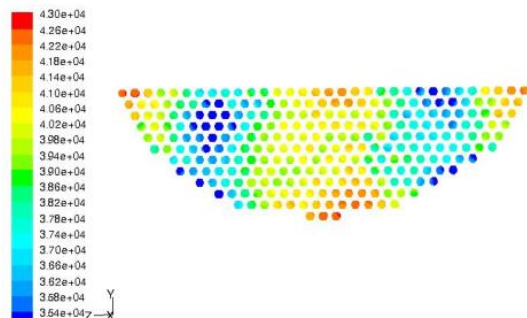


Figure 12. Static pressure inside tubes 30 mm from tube entry

Two “with tube” simulations were conducted where the overall tube pressure drop was reduced to 27 kPa and 16 kPa. Table 1 shows the dependence of tube mass flow rate on overall tube pressure drop for these cases and the original case at 46 kPa. The ratio of minimum to maximum mass flow rate in the tubes varies across the tube sheet with the highest tube pressure drop giving the least variation. In view of the significant dependence of mass flow variation across the tube sheet, simulations were performed with the inertial model instead of Darcy’s law. This led to higher pressure drops and approximately 20% less variation of tube mass flows across the tube sheet.

Flow visualisation by means of vector contours shown on, Figure 14 give a clearer view of the major vortices generated by the side entry of flow. The correlation with flow angle of entry to tubes, Figure 5 and Figure 8 is quite high in the region of the major vortices. The high angles around the outer shell are seen not to be associated with these vortices but are the result of flow along the shell towards the tube sheet and then turning sharply into the nearby tubes.

Sensitivity of results to changes in assumed velocity profiles in the inlet nozzle was tested but found to be only minor when changing from a uniform (top hat) profile to a seventh power law turbulent one.

Large Eddy Simulations

Using the same grids as for the with tubes RANS simulations, large eddy simulations with the dynamic subgrid scale eddy viscosity model of Germano et al (1991) were performed (time-step = $1.0 \times 10^{-4}\text{s}$). Mean flow angles from the LES after 3s of simulation and then over a subsequent 2s of averaging are shown in Figure 13. The asymmetry of flow distributions noted in the above was again seen (although reversed), however the general features of the flows are the same as for the RANS

simulations. LES is arguably the better technique, but is much more numerically intensive since even when used on the same grids as used for the RANS, LES requires much shorter time steps and needs to be run for a significant number of iterations to obtain time averages.

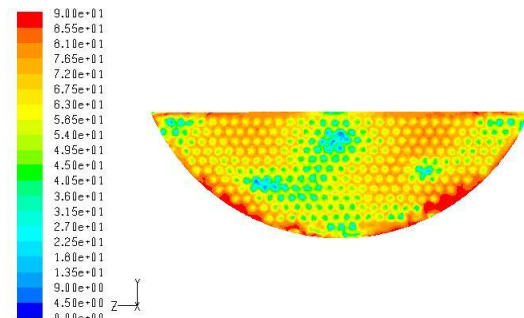


Figure 13. Time averaged flow angle relative to tube axis, 10 mm upstream of tubesheet for LES

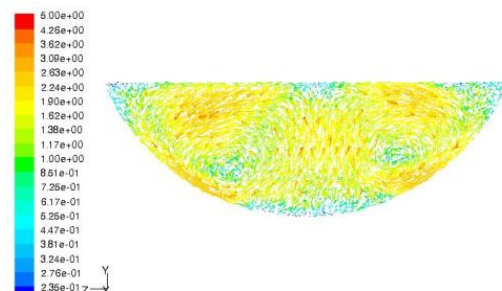


Figure 14. Velocity vectors 10 mm upstream of tubesheet

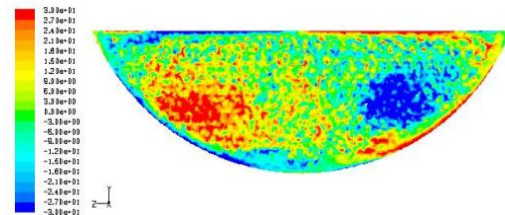


Figure 15. Mean vorticity component along tube axis

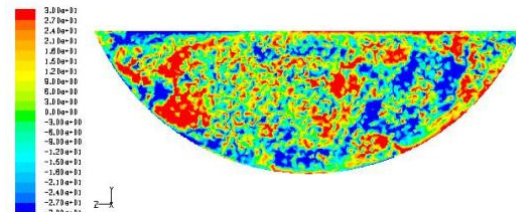


Figure 16. Instantaneous vorticity component along tube axis

Distributions of mean and instantaneous vorticity components along the tube axis, Figure 15 and Figure 16, show the large vortices seen in the RANS simulations and the widespread of this vorticity from one moment to the next due to the vortex flow into some of the tubes at any moment. The significance of the instantaneous vorticity component is that it can show up as localized tube damage at inlets with a spread far larger than suggested from the mean vorticity distributions. The small spatial scale of this vorticity is seen in both the mean and instantaneous views.

Pressure drop across first pass kPa	Ratio of minimum to maximum tube mass flow rate	Standard deviation on average tube mass flow rate – kg.s ⁻¹
16	0.659	0.205
27	0.772	0.125
46	0.864	0.08

Table 1. Dependence of tube mass flow rate on pass pressure drop - average tube mass flow rate = 2.344 kg.s⁻¹

Return Passes in the Heat Exchanger

In view of the extra information given by the “with tubes” approach, the latter was applied to flow from one pass to another. Usually the header shapes for pass-to-pass flows are streamlined and thought to provide little flow disturbance. However, the approximate three to one expansion in area from tubes into the header space leads to significant local flow disturbance which may lead to other spurious effects. Modelling followed the same principles as for the inlet header described above using RANS modelling. For the inlet tubes (flow into header space) a 0.9 m length (27 tube diameters) of each tube was simulated with a uniform velocity distribution assumed at the inlet to this length. The exit tubes were simulated using the “with tubes approach” where the first 0.6 m was free turbulent flow followed by 0.3 m of a porous plug with an inertial resistance of 28 m⁻¹ to give a tube pressure drop of 45 kPa.

Velocity angles, Figure 17, are seen to be very low compared with those of the inlet header flow, except in the vicinity of the shell near the pass separation baffle and the two rows of tube inlets adjacent to the pass separation baffle of the next pass. The reason for these effects can be seen from the pathlines from specific tubes shown on Figure 18, Figure 19 and Figure 20. It should be noted that on these diagrams, the tubes are numbered from left to right starting at the bottom three tubes which are adjacent to the shell

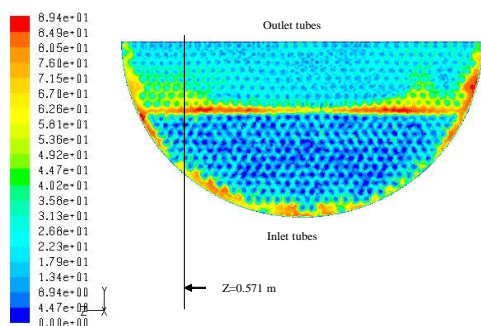


Figure 17. Velocity angles from tube exits to tube inlets of next pass

The pathlines of Figure 18 are from tubes 58 and 68 which are in the middle row and are consistent with expectations of a smooth flow between passes. Flow is from the bottom of the diagram to the top as seen from the tracer injection in one tube which then fans out to several tubes in the next pass. The rapidly expanding jet flow out of each tube is readily seen for one tube (left) but is not so evident with the second tube (right).

Pathlines of Figure 19 are from tubes 242, 256, 264 and 274, which are in the top row adjacent to the pass baffle. The pathlines from tube 274 which is immediately adjacent to the shell shows a severe disturbance of the flow near the shell. On the left side of the diagram, flow is

across the header space while on the right hand side a pattern suggestive of a local vortical structure exists. This structure is certain to become an area where solids will separate out, coalesce and lead to blockages by bridging across tube inlets.

The pathlines of Figure 20, which are from tubes immediately adjacent to the shell (tubes 2, 13, 125 and 152) give further evidence of irregular flow generated by the expansion of individual tube exit flows as well as showing significant flow across the whole header space. Such cross flow is possible only if the full flow segment is simulated and not just one half on the basis of geometric symmetry.

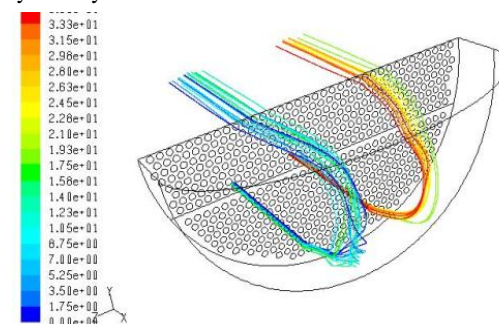


Figure 18. Velocity pathlines from tubes 58 and 68

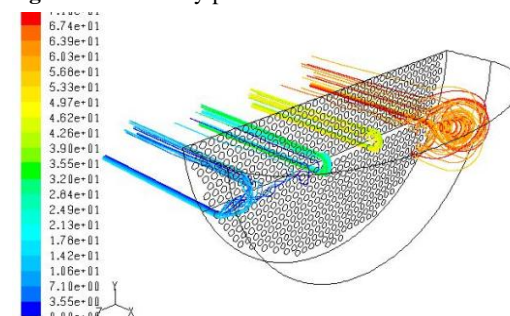


Figure 19. Velocity pathlines from tubes 242, 256, 264 and 274

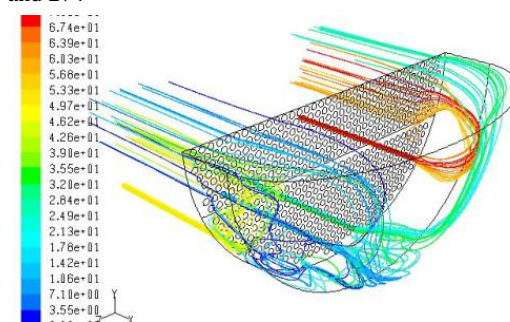


Figure 20. Velocity pathlines from tubes 2, 13, 125 and 152

CONCLUSION

Modelling of side entry shell and tube heat exchanger flow was re-examined by modelling each individual tube and not making use of geometric symmetries. The inertial pressure drop relationship rather than Darcy’s law was found to lead to more uniform flow distributions across the inlet header tube sheet. Asymmetric flow distributions similar in nature to asymmetries noticed in plane expansion flows are observed. Areas of high flow angle into tubes have been found in the inlet header flow and between passes and are restricted to a small region of tubes near the pass separation baffle and the shell. The

rapid expansion of flow from one pass to the next leads to vortical regions where solids, if present, can separate from the flow, coagulate and block tube entries.

REFERENCES

- BREMHORST, K. and LAI, J.C.S., "The role of flow characteristics in corrosion-erosion of tube inlets in the inlet channel of shell and tube heat exchangers". *Wear*, 54, 1, 87-100, May 1979.
- BREMHORST, K. and FLINT, P.J., (1988), "A decade of progress in computational fluid mechanics for solution of industrial problems", *Proceedings Mech 88 - Thermodynamics Conference*, I.E. Aust., Brisbane, 8-13 May.
- BREMHORST, K. and FLINT, P.J., (1989), "Numerical solution of complex flow geometries as an aid to resolving erosion/corrosion problems", *Design against Corrosion, Symposium, Int. Engrs. Aust./Inst. Chem. Engrs.*, Brisbane, April.
- BREMHORST, K. and FLINT, P.J., (1991), "The effect of flow patterns on the erosion/corrosion of shell and tube heat exchangers", *Wear*, 145, 123-135.
- ELVERY, D.G. and BREMHORST, K., (1996), "Erosion-corrosion due to inclined flow into heat exchanger tubes - investigation of flow field", *Proceedings of the ASME Fluids Engineering Division Summer Meeting, San Diego, California, USA July 7-11, FED-Vol. 237*, 595-600.
- GERMANO, M., PIOMELLI, U., MOIN, P. and CABOT, W., (1991), "A dynamic subgrid-scale eddy viscosity model", *Physics of Fluids A*, Vol. 3, 1760.
- MENTER, F. R., (1992), "Improved two equation $k-\omega$ turbulence models for aerodynamics flows", NASA TM-103975.
- WILCOX, D. C., (1998), "Turbulence modelling for CFD", DCW Industries, La Canada, California.
- KEAR, G and BREMHORST, K, (2008a), "Influence of Aeration on the Passivation Characteristics of AS/NZS 3679.1 – 300 Mild Steel in High Temperature Bayer Liquor under Conditions of Disturbed Flow", *Corrosion*, 64, 4, 291-300, April.
- KEAR, G and BREMHORST, K, (2008b), "Application of Pure Oxygen for the Passivation of Mild Steel in High Temperature and Pressure Bayer Liquid under Conditions of Disturbed Flow", *Corrosion Science*, 50, 1962-1970.
- LAI, J.C.S. and BREMHORST, K., (1979), "Control of corrosion-erosion of tube inlets of shell and tube heat exchangers". *Wear*, 54, 1, 101-112, May.
- NEŠIĆ, S, (2006), "Using computational fluid dynamics in combating erosion-corrosion", *Chemical Engineering Science*, 61, 4086-4097.